REVIEW

Review of thermal infrared polarimetry, I: theory

Nathan Hagen*
Utsunomiya University, Department of Optical Engineering, Utsunomiya, Japan

Abstract. We review the physics underlying thermal infrared emission, focusing on the processes that generate polarization. We also discuss a number of features of the theory that are not widely discussed in the literature, including the Straubel theorem for absorbing media, the mixed Poynting vector, and the emission of nonisothermal media. Using a model for emission from nonisothermal media, we present a quantitative discussion of the conditions under which Kirchhoff's law is valid. Using this model, we show how it is possible for many blackbody simulators and infrared camera shutters to produce emission very close to true blackbodies. © *2022 Society of Photo-Optical Instrumentation Engineers (SPIE)* [DOI: 10.1117/1.OE.61.7.070902]

Keywords: infrared; polarization; emissivity; blackbody; Kirchhoff's law; Straubel's theorem.

Paper 20220227V received Mar. 8, 2022; accepted for publication Jul. 5, 2022; published online Jul. 26, 2022.

1 Introduction

Although research in infrared polarization has been pursued at least since Millikan's studies on emission polarization in 1895,[1,2] infrared polarimetry has never reached widespread use. As a result, there are many polarimetric features specific to infrared wavelengths that are not widely known, despite their fascinating physics. This review aims to survey the physics underlying infrared polarimetry and to explore a few of the less common features of the theory.

In the infrared polarization literature, writers often refer to the thermal emission of surfaces, so it is easy to slip into thinking of infrared light emission as a surface phenomenon rather than a volumetric one. A search through the literature encounters "surface emissivity" as a common phrase, and Planck's blackbody law, after all, is generally expressed in terms of surfaces and surface temperatures, rather than volumes and volumetric temperature distributions. Nevertheless, emission is a volumetric property, much like absorption but played out in reverse. For opaque materials, in which absorption completely attenuates incident light after passing only microns deep inside the material, this volumetric behavior is not obvious. For semitransparent (diathermous) materials, however, understanding the volumetric behavior is essential to accurately modeling their emission properties.[3,4]

In Sec. 2, we model the thermal light emission that constantly occurs inside every material and show that the surface emission that we see is simply the portion of that internal light that reaches the surface, transmits, and refracts into the air.[3,5] This model holds even for highly reflective materials such as metals, and we find that the apparent skin-like quality of emission derives from the fact that so many materials in the infrared have strong absorption, so only the layers close to the surface are able to participate in generating the emitted light that we see. In Sec. 6, we also show that emitted light is polarized by the same Fresnel reflection and transmission effects that generate polarization from smooth visible-light surfaces. Because emission polarization is actually antagonistic to reflection polarization, the combination of emitted and reflected light often causes most of the polarimetric signature to cancel, producing the characteristically low degree of polarization values that are typically seen in this regime.[6] In outdoor environments, this cancellation can become small for imaging quite hot surfaces and blue sky (very cold) backgrounds.

The advantage of going carefully through the steps of deriving emission polarization from first principles shows that Kirchhoff's law, which is often presented as an empirical formula, can be derived from basic physics. It also allows us to quantify the range inside which Kirchhoff's

*Address all correspondence to Nathan Hagen, nh@hagenlab.org

law is valid (Sec. 7) and to demonstrate that, although thermal emission may be a totally incoherent process, interference effects still play a role in determining emission properties when thin films (with thicknesses on the order of a wavelength) are present or when using high-resolution spatial/spectral detection.

In addition to improving understanding of the theory, some motivations for pursuing this work are to resolve some questions that are not easily clarified by a casual read through the literature. These questions include the following:

1. If a surface gets wet, with a very thin layer of water, how is its emissivity effected? How thick does the water coating have to be to dominate the surface underneath?
2. Anodized aluminum parts are ubiquitous in optical systems, but if we anodize an aluminum surface, how does the process change its emissivity?
3. How should we model the emissivity of a thin (partially transparent) plastic film?
4. If we paint a surface, how thick should the paint be to obscure the underlying surface? For that matter, why do painted shutters work so well as simulated blackbodies?

In the discussion below, we survey the theoretical tools needed to resolve these questions, though the discussion of anodize layers, and many of the details on paint layers are postponed until Part II of the review. To the extent possible, we aim to provide quantitative answers to these questions and bring together into one place the various work scattered through the literature on these topics. Part II of the review uses these tools to guide analysis of infrared imaging polarization measurements.

2 Calculating Emitted Surface Radiance with the Emission Density, $j(\lambda)$

The first widely known attempt to apply the tools of radiance transfer to the problem of volumetric emission from solids is that of McMahon in 1950.[3] This work was later generalized by Gardon in 1956 to be applied to non-normal angles of emission.[4] Despite its beautiful physics, the resulting model is not well known in the infrared imaging community even though it is widely used in the heat-transfer literature. In the discussion below, we modify the conventional derivation by centering the calculations around radiance rather than optical power. This has the advantage of simplifying expressions while also modernizing the units, so that they are more familiar to the modern reader.

The calculation of the emissivity of an object can be quite involved if presented all at once, so we start with a simple setup and add complexity to the model in stages. At the first stage of the calculation, we aim to calculate the normal-angle emittance of a material with known refractive index $n(\lambda)$ and absorption index $k(\lambda)$, i.e., a complex refractive index of $\tilde{n}(\lambda) = n(\lambda) + ik(\lambda)$. The electric field of a plane wave propagating along z is then written as

$$E = A\,\exp(-i2\pi\tilde{n}(\lambda)z/\lambda)\exp(i\omega t), \tag{1}$$

or

$$E = Ae^{-i2\pi n(\lambda)z/\lambda}e^{-\alpha(\lambda)z/2}e^{i\omega t}, \tag{2}$$

where λ is the wavelength in vacuum and $\alpha(\lambda) = 4\pi k(\lambda)/\lambda$ is the intensity absorption coefficient.

In the discussion below, most variables will have a wavelength dependence. Writing an explicit wavelength dependence, such as $\alpha(\lambda)$, for each variable quickly becomes tedious and makes the equations more difficult to read. As a result, we generally drop the wavelength dependence from intermediate results and include the explicit dependence when it helps to clarify context. In addition, rather than "emitting medium," we generally refer to the region from which we are calculating the emission as "the solid." This simplifies the nomenclature, but readers should note that it can refer to liquids and gases as well, without difficulty.

We start by postulating that the medium is uniform in temperature and composition and has negligible scattering and that each point within the solid can be characterized as emitting isotropic thermal radiation. For highly opaque materials, radiation emitted from within the volume

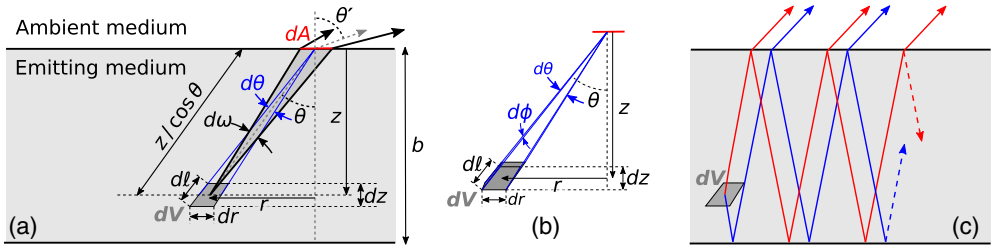

Fig. 1 A plane-parallel slab of partially transparent emitting medium: "the solid." (a) Radiation is emitted from volume dV toward surface element dA, along the ray at angle θ to the surface normal. (b) Geometry of the emission solid angle. (c) Each ray splits into transmitted and reflected components at the top and bottom surfaces. Summing over these secondary rays gives the total light exiting the surface. (c) The red rays are emitted from dV in an initially upward direction, whereas the blue rays are emitted in an initially downward direction.

is quickly absorbed by the surrounding matter and does not reach the surface. For semitransparent materials, however, this volumetric emission j can reach the surface, so calculating the light emitted by the entire solid requires integrating j over the object's volume. The setup for this calculation is illustrated in Fig. 1.

Figure 1 shows the radiation emitted from an element of volume dV in the interior of the solid that reaches a small area element dA of the surface, as originally constructed by Gardon.[4] From this geometry, Gardon develops an integral over dV and the differential solid angle $d\omega$, taking advantage of the conical symmetry of the problem to define dV as a differential sector of a conical annulus. In this way, any region of the solid lying inside the region bounded by the blue lines [with differential angles $d\theta$ and $d\phi$, as indicated in Fig. 1(b)], produces radiation propagating within the same element of the solid angle. The development of the integral is shown in Sec. 10, the end result of which is a simple one-dimensional (1D) integral along the ray between dV and dA.

The quantity $j(\lambda, T)$ is the material's spectral emission density, at a given temperature T, expressed in units of $\mathrm{Wm}^{-3}\,\mathrm{sr}^{-1}\,\mu\mathrm{m}^{-1}$—spectral radiance per unit length. Thus, we can expect that integrating $j(\lambda, T)$ over a length will lead to the familiar spectral radiance $L(\lambda)$ given by the Planck blackbody equation, viz.,

$$L_{\mathrm{bb}}(\lambda) = \frac{2hc^2}{n^2\lambda^5}\frac{1}{e^{hc/(n\lambda k_{\mathrm{B}}T)} - 1}, \quad [\mathrm{Wm}^{-3}\,\mathrm{sr}^{-1}\,\mu\mathrm{m}^{-1}], \tag{3}$$

for Planck constant h, Boltzmann constant k_{B}, and the refractive index of the medium n. The "bb" subscript on L indicates that the radiance corresponds to a blackbody.

In the plane parallel medium shown in Fig. 1, the radiance j is generated in dV, lying at a depth of z below the surface. As it propagates, the emitted light is attenuated by absorption, so only the fraction $\exp(-\alpha z/\cos\theta)$ arrives at the surface. Therefore, the element of radiance dL arriving at the surface from this layer at depth z is

$$dL = je^{-\alpha z/\cos\theta}\mathrm{d}z. \tag{4}$$

By integrating this over the thickness of the slab, from $z = 0$ to $z = b$, we obtain the total spectral radiance arriving at the surface as

$$L = j\int_0^b e^{-\alpha z/\cos\theta}\mathrm{d}z = (1 - e^{-\alpha b/\cos\theta})\frac{j}{\alpha}\cos\theta. \tag{5}$$

We simplify this as

$$L(\lambda, \theta) = \frac{j(\lambda)}{\alpha(\lambda)}[1 - \beta(\lambda, \theta)]\cos\theta, \tag{6}$$

where we define

$$\beta = \exp(-\alpha b/\cos\,\theta), \tag{7}$$

as the bulk internal transmission of the entire slab, and we have assumed that the emission density is uniform throughout the volume. For inhomogeneous materials, or for materials with a temperature that varies throughout the volume, the depth dependence of j prevents it from being pulled out of the integral as a constant.

So far we have ignored any secondary reflections inside the volume: the portion of light that is not transmitted through the upper surface is instead reflected downward, and this radiance is $\rho(1-\beta)(j/\alpha)\cos\,\theta$. After traversing the volume of the slab (and attenuating due to absorption), it reaches the far side of the slab, where it reflects again. Traversing the slab one more time brings it back to the upper surface, where again a portion of the radiation transmits through the surface. This second component is therefore

$$\rho^2\beta^2\tau(1-\beta)\frac{j}{\alpha}\,\cos\,\theta, \tag{8}$$

where ρ^2 is the two internal reflections, β^2 is the attenuation along that doubled path, and τ is the transmission through the surface. This process continues to occur, giving another contribution of

$$\rho^4\beta^4\tau(1-\beta)\frac{j}{\alpha}\,\cos\,\theta, \tag{9}$$

and other higher-order terms. Summing all of these together gives the total upwelling radiance reaching the inside of the surface as

$$L_\uparrow = (1-\beta)\frac{j}{\alpha}\,\cos\,\theta\sum_{n=0}^{\infty}\rho^{2n}\beta^{2n}. \tag{10}$$

So far, we have only considered upwelling emission from the layers inside the slab. Because any thermal emitted radiance is isotropic, there is an equal amount emitted in the downward direction. For this portion, light reaching the upper surface of the slab must first undergo one reflection and suffer attenuation from traversing the volume of the medium, so the first portion of radiance reaching the upper surface is

$$\rho\beta\tau(1-\beta)\frac{j}{\alpha}\,\cos\,\theta. \tag{11}$$

Likewise summing all contributions from multiple reflections, we obtain the total downwelling radiance reaching the inside of the top surface as

$$L_\downarrow = (1-\beta)\frac{j}{\alpha}\,\cos\,\theta\sum_{n=0}^{\infty}\rho^{2n+1}\beta^{2n+1}. \tag{12}$$

The total radiance reaching the underside of the surface is the sum of the upwelling and downwelling terms

$$L = L_\uparrow + L_\downarrow = (1-\beta)\frac{j}{\alpha}\,\cos\,\theta\sum_{n=0}^{\infty}\rho^{n}\beta^{n} = \frac{j}{\alpha}\left(\frac{1-\beta}{1-\rho\beta}\right)\cos\,\theta. \tag{13}$$

If the surface transmittance is $\tau(\lambda)$, the spectral radiance $L'(\lambda)$ that passes through the surface is

$$L' = \tau\frac{j}{\alpha}\left(\frac{(1-\beta)}{1-\rho\beta}\right)\cos\,\theta. \tag{14}$$

Having reached this point, we do not yet know how this emitted radiance L' relates to the standard method of representing surface-emitted radiance, viz.,

$$L_{\text{object}} = \epsilon L_{\text{bb}}. \tag{15}$$

If we consider a material that is highly opaque (large k), then we know that the bulk transmission of the material is approximately zero ($\beta = 0$). In this situation, Kirchhoff's law is unambiguous, giving $\epsilon = 1 - \rho$. In our model of emission from the solid Eq. (14), we use Kirchhoff's law to express the surface transmittance as $\tau = 1 - \rho$. Thus, if we equate our calculated emitted radiance L' Eq. (14) with the familiar form of the object radiance Eq. (15), we have

$$(1-\rho)\frac{j}{\alpha}\cos\theta = (1-\rho)L_{\mathrm{bb}}. \tag{16}$$

At normal incidence, we conclude that

$$\frac{j(\lambda)}{\alpha(\lambda)} = L_{\mathrm{bb}}(\lambda). \tag{17}$$

This means that the emission density divided by the absorption coefficient is equal to the blackbody radiance for the same conditions of wavelength and temperature.

3 Straubel Theorem for Radiance Scaling Across an Interface

So far we have obtained the expression for the emitted radiance L_2 in terms of the internal angle θ_1 but not yet in terms of the external angle θ_2. (Subscript 1 refers to quantities inside the solid, and subscript 2 refers to quantities in the external medium—usually air.) For this, we need to apply the angle-dependent refraction effects at the surface, making use of a well-known theorem in radiometry governing the scaling of the solid angle Ω across an interface [shown in (Fig. 2)], apparently first discovered by Straubel in 1902.[7,8] To start, from Snell's law we know that $n_1 \sin\theta_1 = n_2 \sin\theta_2$. Taking the derivative of both sides with respect to θ_2, this becomes

$$n_1 \cos\theta_1 \frac{d\theta_1}{d\theta_2} = n_2 \cos\theta_2, \tag{18}$$

which leads to

$$\frac{d\theta_1}{d\theta_2} = \frac{n_2 \cos\theta_2}{n_1 \cos\theta_1}. \tag{19}$$

Using the definition of the differential solid angle, $d\Omega_1 = \sin\theta_1 d\theta_1 d\phi$, we also write

$$d\Omega_1 = \sin\theta_1 d\theta_1 d\phi = \frac{n_2}{n_1}\sin\theta_2 d\theta_1 d\phi, \tag{20}$$

so that

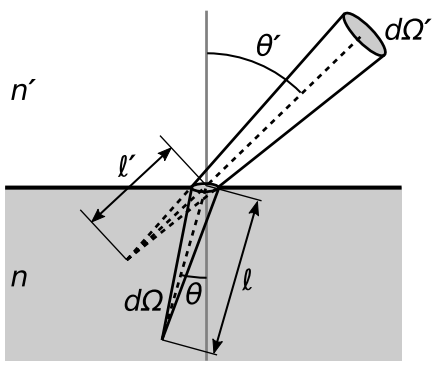

Fig. 2 Refraction of a cone of light, illustrating the geometry of Straubel's theorem.

$$\frac{d\Omega_1}{d\Omega_2} = \frac{\frac{n_2}{n_1}\sin\theta_2 d\theta_1 d\phi}{\sin\theta_2 d\theta_2 d\phi} = \frac{n_2}{n_1}\frac{d\theta_1}{d\theta_2}. \tag{21}$$

Substituting Eq. (19) into this, we obtain

$$\frac{d\Omega_1}{d\Omega_2} = \frac{n_2^2\cos\theta_2}{n_1^2\cos\theta_1}, \tag{22}$$

which is known as Straubel's theorem.

If we ignore for a moment the reflection losses on passing through a smooth interface, then the power entering through an element of solid angle $d\Omega_1$ is equal to the power exiting the interface through $d\Omega_2$:

$$L_2 A d\Omega_2 = L_1 A d\Omega_1. \tag{23}$$

Substituting Eq. (22) into this and incorporate surface transmission loss τ, we have

$$L_2 = \frac{n_2^2}{n_1^2}\left(\frac{\tau(1-\beta)}{1-\rho\beta}\right)L_{\mathrm{bb}}\cos\theta_2. \tag{24}$$

This result, in which the emitted spectral radiance is proportional to the cosine of the exitance angle θ_2, is commonly described as Lambert's cosine law.

As we will see in Sec. 4 below, since the derivation of Straubel's theorem assumes dielectric-only media, the theorem cannot hold in general for absorbing-material interfaces, yet how the theorem should be expressed in the more general case of absorbing media has apparently not been discussed in the literature. The silence on the subject is likely because media with significant k are generally opaque, so they have little transmitted light to measure, making this a case of limited utility for most situations. Likewise, media with small k transmit sufficient light for measurement, but the small value of k minimizes the effect on the refraction angle.

For intermediate cases, we need to use an expression giving the dependence of the refraction angle on the solid's absorption index [given in Eq. (26)].

4 Generalized Snell's Law

When working with absorbing materials, Snell's law is used directly with the complex index $\tilde{n} = n - ik$:

$$\sin\tilde{\theta}_2 = \frac{\tilde{n}_1}{\tilde{n}_2}\sin\tilde{\theta}_1, \tag{25}$$

where we have explicitly labeled each of the complex variables with a tilde. The meaning of a complex-valued angle $\tilde{\theta}_2$ may be unclear, but it is convenient for the purposes of calculating the Fresnel reflection coefficients ρ. However, to get the correct result for emitted light from the solid refracting into an ambient lossless medium (such as air), we can get a better feel for how the complex variables affect the refraction angles by working entirely in terms of real-valued geometry. For an interface between an absorbing emitter (the solid) and a nonabsorbing medium (the ambient air), we have $\tilde{n}_2 = n_2$ and $\tilde{n}_1 = n_1 - ik_1$. For this case, the expression relating the real-valued angle inside the solid to the transmission angle in the ambient is given as

$$\sin\theta_2 = \left(\frac{n_1}{n_2}\sin\theta_1\right)F^{-1/2}, \tag{26}$$

where the Snell's law correction factor F is given by Bell et al. as[9]

$$F = \frac{1}{2}\frac{-a + (a^2 + 4[n_1^2k_1^2 - n_2^2(n_1^2 - k_1^2)\sin^2\theta_2])^{1/2}}{k_1^2 - n_2^2[1 - (k_1^2/n_1^2)]\sin^2\theta_2}, \tag{27}$$

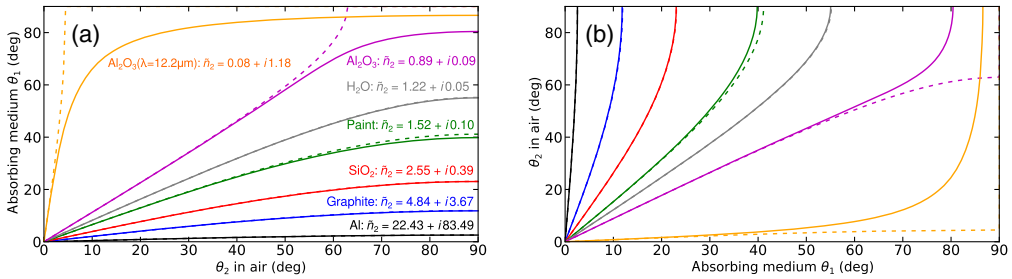

Fig. 3 (a) Curves for θ_2 versus θ_1 refraction going from air $(n_2, k_2) = (1,0)$ into an absorbing medium (n_1, k_1). (b) Curves for θ_1 versus θ_2 going from an absorbing medium (n_1, k_1) into air. For both plots, the solid lines give the generalized Snell's law Eq. (26), and the dashed lines show the standard Snell's law using the real-valued refractive indices alone. Note that the material constants are taken for $\lambda = 10$ μm, except for the alumina curve indicated at 12.2 μm. Refractive indices for each material are obtained from the following references: Al_2O_3,[10] H_2O,[11] SiO_2,[12] graphite,[13] copper,[13] paint,[14] and aluminum.[15]

where $a = n_1^2 - k_1^2 + n_2^2 \sin^2\theta_2$ and is limited to cases in which the ambient medium is non-absorbing $(k_2 = 0)$.

In Fig. 3, a set of curves show the refraction angles given by Eq. (26), drawn together with a second set of dashed curves that are obtained by taking the real parts of $\tilde{n}_1$ and $\tilde{n}_2$ and calculated using the standard Snell's law. We can see that, for angles close to normal (small θ_1, θ_2), the standard Snell's law actually provides a good approximation to the generalized angle calculation. We can also see this mathematically, by taking the approximation $n_2 \sin\theta_2 \ll \{n_1, k_1\}$ in Eq. (27), from which we obtain $F \approx 1$ (where $\{n, k\}$ means "both of n and k"). The approximation is not valid when k_1 is comparable to or larger than n_1.

If we want to know the incident angle θ_1 from within the solid for a given emission angle θ_2, we use Eq. (26) in reverse. Although this produces a transcendental function, this representation of the Snell correction factor is easy to apply due to the smooth monotonic relationship between θ_1 and θ_2 [see Fig. 3(b)]. Unfortunately, however, Eq. (27) does not provide us with the complex form of the angle inside the solid, $\tilde{\theta}_1$, which we need in Sec. 5. The easiest way to get the complex $\tilde{\theta}_1$ is to work out Snell's law Eq. (25) backward, either using a nonlinear solver or by interpolation.

5 Polarization and the Complex Fresnel Equations

So far, all of our expressions for the emitted radiance and emissivity of the solid have been written in terms of the Fresnel intensity coefficients for surface transmittance τ and reflectivity ρ. The Fresnel coefficients are more often written in terms of complex amplitudes t and r, from which the intensity coefficients are derived as $\rho = rr^*$ and a similar expression for the transmission. (The $*$ superscript indicates a complex conjugate.) The most general form of the complex-valued Fresnel reflection and transmission, written for p-polarized light (electric field vibration in the plane of incidence at the surface) and for s-polarized light (electric field vibration perpendicular to the plane of incidence), are written as[16,17]

$$\tilde{r}_\mathrm{p} = \frac{\tilde{n}_2 \cos\tilde{\theta}_1 - \tilde{n}_1 \cos\tilde{\theta}_2}{\tilde{n}_2 \cos\tilde{\theta}_1 + \tilde{n}_1 \cos\tilde{\theta}_2}, \quad \tilde{r}_\mathrm{s} = \frac{\tilde{n}_1 \cos\tilde{\theta}_1 - \tilde{n}_2 \cos\tilde{\theta}_2}{\tilde{n}_1 \cos\tilde{\theta}_1 + \tilde{n}_2 \cos\tilde{\theta}_2}, \tag{28}$$

and the corresponding surface transmission amplitude coefficients are,[17]

$$\tilde{t}_\mathrm{p} = \frac{2\tilde{n}_1 \cos\tilde{\theta}_1}{\tilde{n}_2 \cos\tilde{\theta}_1 + \tilde{n}_1 \cos\tilde{\theta}_2}, \quad \tilde{t}_\mathrm{s} = \frac{2\tilde{n}_1 \cos\tilde{\theta}_1}{\tilde{n}_1 \cos\tilde{\theta}_1 + \tilde{n}_2 \cos\tilde{\theta}_2}. \tag{29}$$

Taking the magnitude squared of r and t, respectively, we obtain the intensity reflectivity and transmittance as[18–21]

$$\rho_p = \tilde{r}_\mathrm{p}\tilde{r}_\mathrm{p}^*, \quad \rho_\mathrm{s} = \tilde{r}_\mathrm{s}\tilde{r}_\mathrm{s}^*, \tag{30}$$

and

$$\tau_\mathrm{p} = (\tilde{t}_\mathrm{p}\tilde{t}_\mathrm{p}^*)\frac{\mathrm{Re}\{\tilde{n}_2\ \cos\ \tilde{\theta}_2^*\}}{\mathrm{Re}\{\tilde{n}_1\ \cos\ \tilde{\theta}_1^*\}}, \quad \tau_\mathrm{s} = (\tilde{t}_\mathrm{s}\tilde{t}_\mathrm{s}^*)\frac{\mathrm{Re}\{\tilde{n}_2\ \cos\ \tilde{\theta}_2\}}{\mathrm{Re}\{\tilde{n}_1\ \cos\ \tilde{\theta}_1\}}. \tag{31}$$

The fraction at the rightside of τ_p and τ_s in Eq. (31) expresses the change in the beam cross-sectional area upon refraction.

For unpolarized light, it is common to define an unpolarized average reflectivity ρ_a given as

$$\rho_\mathrm{a} = \frac{1}{2}(\rho_\mathrm{p} + \rho_\mathrm{s}). \tag{32}$$

Because thermally emitted light from thick media is typically incoherent, the phase relationship between s and p reflected light can be considered random, that is, emitted radiance is generally partially linearly polarized, but not elliptically polarized, for thick media.

An example set of reflectivity curves is shown in Fig. 4, at $\lambda = 10\ \mu$m, for the cases of light incident from air and reflecting from an absorbing medium. Thus, in this case, $\tilde{n}_1 = n_1$ and $\tilde{\theta}_1 = \theta_1$. Note that, although the water reflectivity curve looks like a curve for a nonabsorbing interface, it does not have a true Brewster angle.[22] Instead, it has a pseudo-Brewster angle (for $\lambda = 10\ \mu$m) at an external angle of incidence of $\theta_2 = 50.6$ deg, where $\rho_\mathrm{p} = 4.2 \times 10^{-4}$.

A difficulty with using the complex Fresnel equations in our situation is that the radiance transfer approach allows us to know θ_1 inside the solid, but it does not tell us the corresponding value for $\tilde{\theta}_1$. If we naively attempt to use θ_1 in place of $\tilde{\theta}_1$ in Eqs. (28) and (29), we will obtain unphysical reflection and transmission coefficient values. Thus, if we invert Eq. (27) for the generalized Snell's law, we can calculate the correct angle of emission from the solid. Instead, we must invert Eq. (25) to obtain the corresponding complex angle $\tilde{\theta}_1$ for use in the Fresnel equations.

Another phenomenon that may be unfamiliar to many is that, for absorbing incident media, interference between the incident wave and reflected wave causes nodes in the intensity distribution near the material interface, and this alters the behavior at the interface.[23,24] As a result, the energy conservation requires the expression

$$\tau + \rho + \mu = 1, \tag{33}$$

where μ can be positive or negative. This extra μ term, which has been termed the "mixed Poynting vector," becomes negative when a maximum node (intensity peak) occurs near the

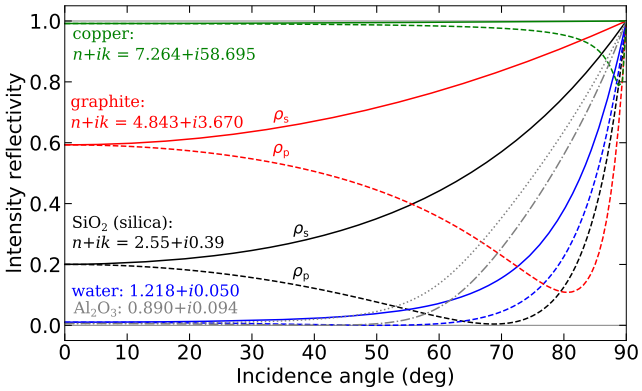

Fig. 4 Fresnel surface reflectivity Eq. (30) as a function of angle of incidence, for light incident from air onto five different polished materials, at 10 μm wavelength. Solid curves: s-pol, dashed curves: p-pol. Refractive indices for each material are obtained from the following references: Al_2O_3,[10] H_2O,[11] SiO_2,[12] graphite,[13] and copper.[13]

interface itself and positive when a minimum node (intensity valley) occurs near the interface, causing a small increase or decrease in the amount of transmitted light depending on whether the node at the interface is a valley or a peak. This extra term is written as[25,26]

$$\mu_{\mathrm{p}} = (\tilde{r}_{\mathrm{p}}^{*} - \tilde{r}_{\mathrm{p}})\frac{\tilde{n}_1^{*}\cos\tilde{\theta}_1 - \tilde{n}_1\cos\tilde{\theta}_1^{*}}{\tilde{n}_1^{*}\cos\tilde{\theta}_1 + \tilde{n}_1\cos\tilde{\theta}_1^{*}}, \quad \mu_{\mathrm{s}} = (\tilde{r}_{\mathrm{s}}^{*} - \tilde{r}_{\mathrm{s}})\frac{\tilde{n}^{*}\cos\tilde{\theta}_1^{*} - \tilde{n}_1\cos\tilde{\theta}_1}{\tilde{n}_1^{*}\cos\tilde{\theta}_1^{*} + \tilde{n}_1\cos\tilde{\theta}_1}, \tag{34}$$

which at normal incidence simplifies to[27]

$$\mu_{\theta_1=0} = \frac{4k_1(n_1k_2 - n_2k_1)}{n_1|\tilde{n}_1 + \tilde{n}_2|^2}. \tag{35}$$

Researchers who discuss the mixed Poynting vector almost universally assert that μ is "small" and therefore can be neglected.[28–31] However, if one proceeds to substitute n, k values for example materials into Eq. (34), one quickly finds that μ can be surprisingly large in the thermal infrared domain for a wide class of materials. It is quite common for metals to have $n < 1$, and in this regime, it is not unusual to have $|\mu| > 1$ (i.e., transmission >200%) at higher angles of incidence, as shown in Fig. 5. Thus, what is missing from the literature is a description of the correct context for calling μ "small."

Figure 5 shows example curves of $\mu(\theta)$ for light transmitted across an interface from an absorbing medium (in this case, silica and alumina) into air. For silica, we see that μ is small ($|\mu| < 0.019$), but it seems careless to refer to even a 2% change as negligible, especially as it occurs at normal incidence and not just at large angles of incidence. For alumina, the larger ratio between the absorption and refractive indices means that μ plays a larger role. Although $\mu = -0.011$ at normal incidence, it reaches $\mu_{\mathrm{p}} = -1.14$ and $\mu_{\mathrm{s}} = -2.62$ at an angle of incidence $\theta' = 79$ deg. This does not violate Eq. (33) because we also find that $\tau_{\mathrm{p}} = 1.75$ and $\tau_{\mathrm{s}} = 3.08$ there.

From these results, we can conclude that the nonlinear interaction between the incident wave and reflective wave at the interior boundary of the solid causes an enhancement (or in other cases, diminishment) of the internally reflected wave intensity. Because the absorption coefficient of these materials is large, this enhancement will be small in comparison with the absorption experienced by the wave as it propagates back toward the interior of the solid. For all but the thinnest of films, this likely makes the effect difficult to observe using the standard experimental approach of taking the ratio between the incident light and the transmitted light. However, semitransparent (and thus extremely thin) metal coatings on mylar films may provide the right combination of circumstances to observe this effect.

However, as we see in Eq. (36), the surface transmittance is proportional to the object's emittance. This means that any impact that the mixed Poynting vector has on the surface transmittance should be observable as a change in emittance. Either this impact has not been observed before, due to the limited range of wavelengths and angles over which it generally occurs,

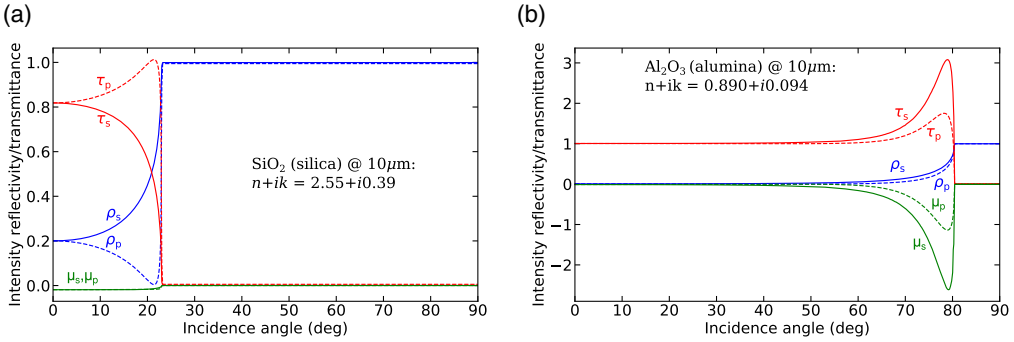

Fig. 5 Fresnel intensity reflection $\rho(\theta)$, transmission $\tau(\theta)$, and modulation $\mu(\theta)$ terms, calculated for light emitted into air from within (a) silica and (b) alumina, using Eqs. (30), (31), and (34). The refractive indices used here are the same as in Fig. 4.

or the impact is negligible, for reasons that are not considered in the existing literature. Either case provides tasks for future work.

6 Emissivity

The emissivity is defined as the emitted radiance of a body in proportion to the emitted radiance of an equivalent (same temperature and same angle) blackbody emitter, so with Eq. (24) our radiative model gives the spectral emissivity as

$$\epsilon_{\mathrm{m}}(\lambda,\theta_2)=\frac{L_{2,\mathrm{m}}(\lambda,\theta_1)}{L_{\mathrm{bb}}(\lambda,\theta_1)}=\frac{L_{2,\mathrm{m}}(\lambda,\theta_1)}{L_{\mathrm{bb}}(\lambda)\cos\theta_2}=\tau_{\mathrm{m}}(\lambda,\theta_2)[1-\beta(\lambda,\theta_2)]. \tag{36}$$

Here, "m" is used to index the polarization state as either p or s. When the solid is optically thick, so that as $\beta\to 0$, we can see that this equation simplifies to $\epsilon_{\mathrm{m}}=\tau_{\mathrm{m}}$—the emissivity of the object is equal to the object surface transmittance. This is from the perspective of light generated from inside the solid, refracting through the surface. On the other hand, we can look from the perspective of light in air incident on the surface of the solid. For an opaque solid, all light transmitted through the surface is absorbed, so this is also equivalent to $\epsilon_{\mathrm{m}}=\alpha_{\mathrm{m}}$, which is the basic expression of the Kirchhoff law. Figure 6 shows curves obtained from Eq. (36) for water, Al_2O_3 (alumina), SiO_2 (silica), graphite, and copper.

At normal angles, when the ambient medium is air ($n_2=1$, $k_2=0$), the emissivity Eq. (36) simplifies to

$$\epsilon=\frac{4n_1}{(n_1+1)^2+k_1^2}, \tag{37}$$

which is shown in Fig. 7. The curve for $k_1=0$ may appear to be nonphysical because a non-absorbing medium cannot be an emitter, but this result can be taken as an asymptotic limit of a medium in which k_1 is brought closer to zero, whereas the medium itself becomes semi-infinite in extent. If the limit is taken in this way, k_1 can be brought arbitrarily close to zero, if not quite all of the way to zero.

From Eq. (27), we can calculate the incident angle θ_1 from the emission angle θ_2, and by inverting Eq. (25) we can calculate the complex angle $\tilde{\theta}_1$ that is needed for the general Fresnel equations Eq. (31). Because $\beta=\exp(-\alpha b/\cos\theta_1)$ is a function of the material thickness b, we find that, for small values of thickness, ε increases approximately linearly with b, but that as b becomes large, β approaches zero, and the emissivity approaches an asymptotic value. Following Edalatpour, we can define a "critical thickness" b_{c} at which the emissivity reaches 99% of its asymptotic value.[33] Taking the logarithm of Eq. (7)

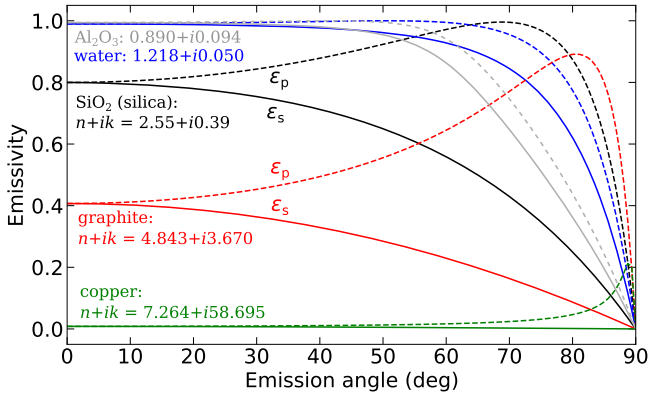

Fig. 6 Fresnel emissivity Eq. (36) as a function of angle of emission, for light emitted into air, from air onto five different polished materials, at 10 μm wavelength. Each material is assumed to be thick enough that $\beta\approx 0$. Solid curves: s-pol, dashed curves: p-pol. The refractive indices used here are the same as in Fig. 4.

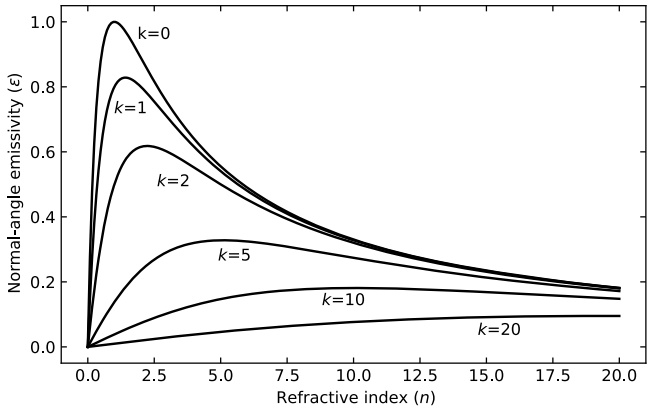

Fig. 7 Normal-angle emissivity of light emitted into air, for various (n, k). (Adapted from Ref. 32.)

$$b_c(\lambda) = 4.6\frac{\lambda \cos\theta_1}{4\pi k_1(\lambda)}, \tag{38}$$

for $4.6 \approx \ln(0.01)$. In the thermal infrared (3 to 15 μm), typical values for k_1 in metals are 30 to 90,[34] giving critical thicknesses of 24 to 360 nm (i.e., less than a micron). Many nonmetal absorbing materials have $0.05 < k_1 < 5$,[35] giving $b_c = 0.44$ to 220 μm (i.e., well under 1 mm).

In the outdoors, the surfaces exposed to water tend to be hydrophilic, so water tends to completely wet the surface as a film rather than drawing together into beads. This includes most glasses and ceramics and the most common metals (aluminum, steel, copper, etc.).[36] After being saturated with rainwater and allowed to drain, many surfaces tend to retain a thin water film of roughly 3 μm thickness.[37] Because water at $\lambda = 4$ μm and 10 μm has absorption indices of $k_1 = 0.0046$ and 0.051, the critical thicknesses at which the water completely obscures the emission and reflection of the underlying surface is about $b_c = 0.8$ mm. This thickness is only achieved as a layer fully covering a surface when the water cannot fully drain, so we expect that most wet surfaces are not fully obscured by their overlying water films.

6.1 *Emission from Films and Coatings*

Although Eq. (36) allows us to calculate the emissivity at any angle of incidence, for a homogeneous material, many materials naturally form a surface oxide layer upon exposure to air. Pure aluminum, for example, produces a natural amorphous oxide layer that is typically 2 to 4 nm thick.[38] Naturally, the question arises about how these surface layers modify the appearance of these materials in the infrared. For nontransparent coatings, the object will take on the optical properties of the coating material if the layer is very thick. Conversely, it will maintain the optical properties of the substrate if the coating is quite thin. To define "thick" and "thin" for this usage, we once again make use of the critical thickness b_c of the coating material to make a good approximation.

References 39 to 41 develop a model for going beyond the approximate answer that we suggest here, for the case of transparent surface layers. For many coating layers, the coherence length of blackbody spectra exceeds the coating thicknesses. As a result, even though the emission of the substrate is incoherent, interference effects produced by multiple reflections within the surface layer will modify the coating optical properties. Modeling this requires the use of a coherent-light model that tracks the phase of a light wave passing through the coating, closely resembling the approach typically found in thin film optical models at shorter wavelengths. The resulting model accurately reproduces the modulations seen when monitoring the emissivity of a film as it is being grown on top of a substrate (as in Fig. 8).

A general approach that allows for the thickness of the film to be of the same order as the coherence length of the emitted light requires use of a partial coherence theory of thin film optics.[42,43] Such a partial coherence theory allows one to go smoothly between the coherent and incoherent extremes. We can also note that, although thermal emission is incoherent (has a very

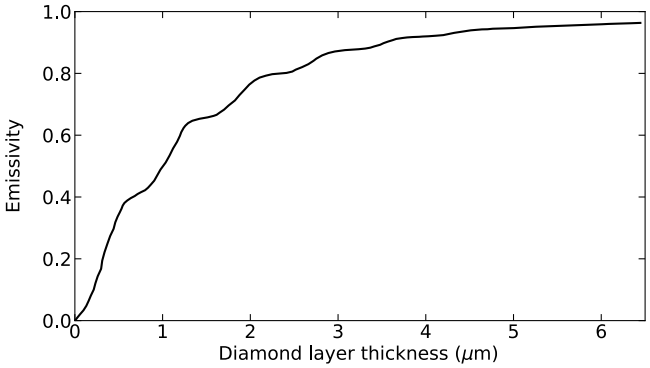

Fig. 8 Oscillations in the normal-angle emittance of a surface film as a function of the film thickness, shown for a diamond film on a silicon substrate, measured for $\lambda = 2.3$ μm at a temperature of 1073 K. (Data obtained from Ref. 33).

short coherence length), the appropriate coherence length to use when modeling a measurement is also determined by the angular size of the detection aperture and the spectral bandwidth of detection, rather than solely by the size and spectrum of the source alone. For small solid angles and narrow spectral bandwidths, even thermal light becomes coherent.

Although a model of a transparent coating on an absorbing substrate is quite useful, transparent coatings are somewhat rare among materials in the thermal infrared. Most coatings, such as the natural oxide coatings that form on many metals upon exposure to air, are partially transparent and partially absorbing/emitting. To model this more general case, it is necessary to augment the coating model to include not only interference of partial reflections but also absorption and incoherent emission within the film. This is the approach taken in Ref. 33, which models the effect of growing a thin metal film or an absorbing dielectric film on top of an absorbing substrate. As we should expect, the model shows a continuous transition from the optical properties of the substrate to those of the film as the film increases in thickness. The change is most rapid when the film is at its thinnest and asymptotically approaches its final value when the film thickness exceeds b_c (see Fig. 8). As with the transparent film, we also find oscillations in the emissivity curve as a function of thickness or wavelength.

7 Refining Kirchhoff's Law

The basic form of Kirchhoff's law expresses the equivalence of emission and absorption: $\epsilon_m(\theta, \phi, \lambda) = \beta_m(\theta, \phi, \lambda)$ for polarization state m. In most of the literature, the conservation of energy for the interaction of light with media is invoked to say that probabilities of reflection, transmission, and absorption sum to 1: $\rho^\circ_m + \tau^\circ_m + \beta^\circ_m = 1$. Using the equivalence property of emission and absorption, this leads to the form of Kirchhoff's law most commonly used in thermal imaging:

$$\epsilon^\circ_m = 1 - \rho^\circ_m - \tau^\circ_m. \tag{39}$$

The superscript $^\circ$ is used to indicate that these are properties of the object (apparent properties) and not just a single surface (surface properties). For opaque media, $\tau^\circ = 0$, in which case Eq. (39) provides a simple method for obtaining the emissivity from the reflectivity ρ°.

In the literature, Kirchhoff's law is more often written as $\epsilon_m = 1 - \rho_m - \tau_m$, i.e., with the Fresnel coefficients ρ and τ rather than the apparent object reflectivity and transmittance. Doing so, however, ignores the effect of internal reflections within the object and internal scattering, so it is strictly only true for either opaque $\tau^\circ = 0$ or diaphanous ρ° media. In addition, there is also a common assumption that, because the interface is an infinitesimally thin region, no absorption is possible at the surface. If true, this would allow the surface transmittance to be calculated from the complement of the reflectivity when the emissivity is negligible, $\tau = 1 - \rho$. However, for absorbing media in which the waves are incident from within an absorbing medium,

we have seen that there can also exist a small amount of (positive or negative) "apparent surface absorption" μ.

A weakness of using the Kirchhoff law for deriving ϵ from ρ is that its validity can be unclear for inhomogeneous media and particularly for nonisothermal media. The direct approach of modeling the emissivity from the spectral emission density $j(\lambda)$ provides better insight into the physical behavior.

Using the incoherent sums of partial waves within the solid, McMahon derived expressions for the normal-angle emissivity, reflectivity, and transmittance as[3]

$$\left.\begin{aligned}\epsilon_m(\lambda,\theta_1) &= \tfrac{\tau_m(1-\beta)}{1-\rho_m\beta}\\ \rho^\circ_m(\lambda,\theta_1) &= \rho_m\left[1+\tfrac{\beta^2(1-\rho_m)^2}{1-\rho_m{}^2\beta^2}\right]\\ \tau^\circ_m(\lambda,\theta_1) &= \beta\rho_m\left[\tfrac{(1-\rho_m)^2}{1-\rho_m{}^2\beta^2}\right]\end{aligned}\right\}, \tag{40}$$

where ρ° and τ° are the apparent spectral reflectivity and spectral transmittance of the object, respectively, and ρ and τ retain their meaning as the Fresnel intensity reflectivity and transmittance of the interface between the solid and the ambient medium, respectively. The wavelength and angle dependence of ρ and β were suppressed for clarity. Adding all three together, with some algebra we obtain the Kirchhoff law

$$\epsilon_m(\lambda,\theta_1)+\rho^\circ_m(\lambda,\theta_1)+\tau^\circ_m(\lambda,\theta_1)=1. \tag{41}$$

Thus, for a homogeneous and isothermal medium, we have been able to derive Kirchhoff's law as a consequence of the Fresnel equations, for all angles and all polarization states. One difference in Eq. (40) from McMahon's results is that the expression for ϵ_{m} uses τ_{m} in place of McMahon's $(1-\rho_{\mathrm{m}})$. These are usually asserted to be equivalent, but we have seen from Eq. (33) that, although they are typically close, they are not exactly equivalent due to the presence of the mixed Poynting vector term μ. Thus, it seems that the mixed Poynting vector may point to a deviation from Kirchhoff's law, for situations in which μ is significant.

7.1 *Nonisothermal Media*

Treatments of Kirchhoff's law generally state that the law is valid when the emitting object is in local thermodynamic equilibrium (LTE) and may further add that this is not satisfied when an object is not isothermal. Because LTE is never exactly satisfied in practice, it is even more important to be able to say quantitatively to what degree a given situation permits the law to provide accurate results, that is, rather than evaluating a situation as valid or invalid for applying the law, we should instead express how closely we can expect the law to hold. First, we start with a heuristic analysis to gain insight into the shape of the problem before going on to developing the path integral for the nonisothermal case.

We can start with an example of a painted metal plate that is exposed to the open air and is cooled by air convection currents and radiative losses. The paint coating has an absorption index of $k_1 = 0.47$ at wavelength $\lambda = 10$ μm. In this case, the skin depth of the coating is $\alpha^{-1} = \frac{\lambda}{4\pi k_1} = 1.7$ μm. Regardless of the status of Kirchhoff's law, we can expect that most of the emission from the solid will take place within this narrow region just below the surface. If the paint layer is nonisothermal, then any thermal gradient will have to be significant within this skin depth. Because most paint coatings are 5 to 200 μm thick, this narrow region is the outermost surface of the paint. If the temperature difference between the warm plate (the "substrate" of the coating) and the surface of the coating is 5°C and the coating is 100 μm thick, then the temperature delta across the skin depth is only $5\ \mathrm{K} \times (0.7\ \mu\mathrm{m}/100\ \mu\mathrm{m}) = 35$ mK. This gives the maximum possible effect that the thermal gradient within this coating can have on the emissivity, making the surface appear as if it were 35 mK warmer than it really is. In practice, the emission by deeper layers is attenuated by absorption before reaching the surface, so the change in emission is even smaller than this and therefore below the noise level of most thermal infrared imagers. With this result in mind, we can say that painted metal surfaces used as blackbody

simulators will likely have an apparent radiative temperature that differs by less than ~35 mK from the temperature of the underlying metal substrate as long as the high-emissivity coating layer is kept to thicknesses near 10 μm.

To make this more quantitative, we develop a model for the emission of a nonisothermal solid. The spectral emission density j becomes a function of z due to the linear depth-dependence of temperature within the solid: $T = T_s + \gamma z$ for surface temperature T_s and temperature gradient γ (in units of K/μm), so

$$j(\lambda) = \frac{2hc^2}{\lambda^5} \frac{\alpha(\lambda)}{\exp[hc/\lambda k_B(T_s + \gamma z)] - 1}. \tag{42}$$

Inserting this into Eq. (4) gives the element of radiance dL emitted from within a layer of thickness dz (see Fig. 1). Integrating this over the thickness of the solid, from $z = 0$ to $z = h$, we obtain the spectral radiance arriving at the surface as

$$L = \frac{2hc^2\alpha}{\lambda^5} \int_0^b \frac{e^{-\alpha z/\cos\theta}}{\exp[hc/\lambda k_B(T_s + \gamma z)] - 1} \mathrm{d}z. \tag{43}$$

Although this is a complicated integral, the expression

$$f(z) = (\exp[hc/\lambda k_B(T_s + \gamma z)] - 1)^{-1} \tag{44}$$

is close to linear when the gradient term is small in comparison with the surface temperature, $\gamma z \ll T_s$. If we take the Taylor series expansion of this expression about the point $\gamma = 0$, then we obtain

$$f(z) = \left(\frac{1}{e^{a/T_s} - 1}\right) + \left(\frac{a\gamma z e^{a/T_s}}{T_s^2(e^{a/T_s} - 1)^2}\right) + \ldots \tag{45}$$

for $a = hc/\lambda k_B$. Putting this expansion into Eq. (43), we obtain

$$L = L_{iso}\left[1 + \left(\frac{\gamma hc}{\alpha\lambda k_B T_s^2} \frac{\cos\theta}{1 - e^{-a/T_s}}\right)\left(1 - \frac{\alpha b\beta}{\cos\theta(1-\beta)}\right)\right], \tag{46}$$

where L_{iso} is the radiance obtained for an isothermal solid at T_s. When the solid is semi-infinite in extent ($b \to \infty$), then this simplifies to

$$L = L_{iso}[1 + M], \tag{47}$$

where

$$M(\theta) = \left(\frac{\gamma hc}{\alpha\lambda k_B T_s^2}\right) \frac{\cos\theta}{1 - e^{-hc/(\lambda k_B T_s)}} \tag{48}$$

is the nonisothermal modifier term. Although following a different derivation, this last result agrees with that given by Ref. 44. We can note that $M \propto 1/\alpha$, so that materials with large absorption index k tend to have values closely agreeing with L_{iso} unless the thermal gradient is extreme.

Figure 9 shows example curves of $M(\theta)$ for different paint coating thicknesses from 2 to 200 μm and a temperature difference $\Delta T = 4$°C between the two sides of the coating (the upper surface exposed to air and the lower surface touching the substrate). For very thin layers of paint that still have a thermal delta of 4°C, we see that the nonisothermal effect on the emittance can reach as high as 10%. However, for more ordinary thermal deltas, the value of M quickly goes below our ability to measure.

Because there is a wide variety of base media and additives in paints, there is a corresponding wide range of refractive and absorption indices. Oppenheim gives a representative measurement of $(n_1, k_1) = (1.52, 0.46)$, whereas Richmond gives $(n_1, k_1) = (1.4, 0.01)$, and Tyo finds $(n_1, k_1) = (1.6, 0.1)$.[6,14,45] These values fall within the range of our own experimental measurements, in which the high-k paints generally contain a large number of pigment particles, making

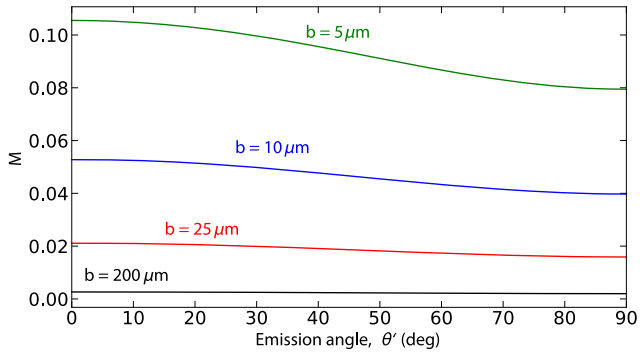

Fig. 9 Emission modifier M, calculated from Eq. (48) for different thicknesses b of paint coatings, assuming $(n_1, k_1) = (1.52, 0.1)$, and a temperature difference of 4°C across the coating.

them appear black in the visible spectrum. The paint layers simulated in Fig. 9 assume intermediate values of $(n_1, k_1) = (1.52, 0.1)$.

In addition to the requirement that the emitting object be isothermal, one sometimes encounters the statement that the object must also be homogeneous for Kirchhoff's law to hold.[41] However, it is clear that inhomogeneous objects do not by themselves cause a violation of the equilibrium condition for Kirchhoff's law because Kirchhoff's law has been applied successfully to multilayer films and to composite materials such as concrete.

7.2 *Nonisothermal Behavior in Paints and Glasses*

Figure 9 shows that a 4°C temperature difference across any paint coating more than 5-μm thick produces such a small change in emissivity that it will be difficult to measure. Although this simulation assumes a temperature delta of 4°C, the author's experience with thin paint coatings in the lab indicate that deltas of 0.2°C to 0.5°C are more likely (using contact thermisters to measure substrate and coating surface temperature). As a result, for blackbody simulator paint coatings, we should be able to neglect the effect of deviating from isothermal sources.

If the thermal gradient becomes steeper and the absorption coefficient k becomes smaller (so that deeper regions participate in emission), the change in emissivity can become significant. For example, for a coating layer with $k = 0.009$, a temperature delta of 2°C across a layer of 5 μm thickness (i.e., a gradient of $\gamma = 0.4$ K/μm) produces a 1.5% change in emissivity at normal incidence, falling off to 1.2% near the grazing incidence.

We can see from Eq. (48) that M is proportional to the thermal gradient γ and inversely proportional to the absorption index k. Thus, M increases linearly with the thermal change ΔT across the emitter's skin depth. If we scale M by k/γ, then we can use the same curve for all values of k, ΔT, and b, as shown in Fig. 10. The proportionality $M \propto \gamma/k$ also shows why

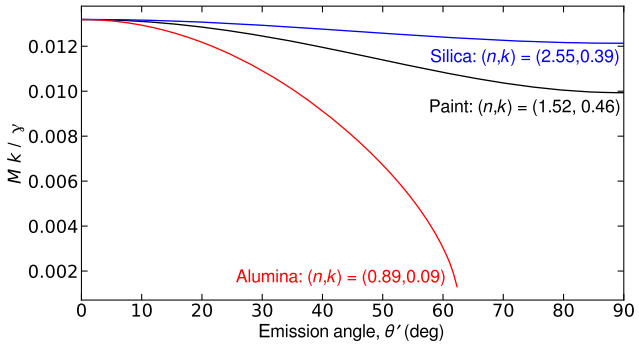

Fig. 10 If the refractive index is held constant, the scaled modifier Mk/γ produces one curve for all different absorption indices k and different thermal gradients γ (i.e., all of the curves of Fig. 9). The curves shown here are calculated from Eq. (48), with the k-values included in the curve labels for ease of reference.

metals present no difficulty for Kirchhoff's law—the large k value and low γ of most metals make M negligible in almost all circumstances.

Using the curves shown in Fig. 10, we can interpret the results in the following way. The blue curve shows that, if there is a 4°C temperature difference between the substrate and the surface of the coating layer, for the coating layer thickness of 10 μm, then the deviation of emission from the isothermal case will be about 5%. One can likely achieve these kinds of conditions by heating the substrate to a high temperature (such as 100°C using the painted kitchen pot shown in Fig. 3 of Part II of this review) while cooling the surface with a fan blowing cool air. This illustrates the conditions under which the nonisothermal effect becomes important.

In the case of silica (SiO_2) and alumina (Al_2O_3) glasses, the emission skin depth at $\lambda = 10$ μm is 2.0 and 0.9 μm, respectively. For alumina, however, 10 μm happens to be close to an absorption peak, so it is not necessarily representative of the material's overall behavior in the thermal infrared. In the midwave infrared (MWIR) (3 to 5 μm), for example, the absorption coefficient for silica drops to $k = 0.00035$—three orders of magnitude lower than the value at 10 μm. Similarly, the absorption index for alumina drops to 0.0018 and for paint (if we take polymethyl methacrylate as representative of a plastic-based paint) to 0.00065. Thus, in the MWIR at $\lambda = 4$ μm, the skin depths of silica, alumina, and acrylic-base paint become 2.3, 0.5, and 1.2 mm, respectively. The lower absorption coefficients in the MWIR versus longwave infrared (LWIR) mean that nonisothermal effects will be more likely in the midwave regime.

Although most natural materials, under normal circumstances, do no deviate significantly from Kirchhoff's law, one category of natural materials that consistently exhibits significant departures from Kirchhoff's law is layered fine particulate such as quartz sand powder.[46] Reference 46 measured up to 6% deviations from Kirchhoff's law for dry unpacked quartz dust. The air gaps between particles reduce the thermal conductivity of the material while preventing convective cooling; at the same time, this allows for sunlight to penetrate deeply and heat up the underlying particle layers, producing a large thermal gradient. Another material having similar behavior is lunar soil.[47,48] One might expect fresh snow to have similar properties, due to having a similar physical structure, but experimental measurements have shown that snow exhibits a close correspondence to Kirchhoff's law.[49]

One can of course envisage cases in which nonisothermal behavior has a predominant effect on emission. For example, most "transparent" materials in the infrared actually have a small amount of absorption present. We can imagine a thick slab of such a medium, in which the slab thickness is larger than the material's thermal penetration depth, but much shorter than the optical absorption depth. Within such a thick slab, emission can take place over a large range of distances, allowing the various emitting layers to have large differences in temperature.

7.3 *Kirchhoff's Law for Gases*

When modeling gases in the thermal infrared, it is common to write Kirchhoff's law simply as absorption equals emission: $(1-\beta) = \epsilon$. Although one can interpret this as equivalent to Eq. (41) when the reflectivity is zero and the transmission is $(1-\beta)$, equating absorption and emission is actually the most fundamental form of Kirchhoff's law.[50] As a result, it is not necessary to know the scattering (the diffuse reflection) by the gas cloud to calculate the emission. Instead, one needs to know only the gas temperature T_{gas} and its absorbance χ along the relevant line of sight. For a gas cloud of thickness ℓ along the line of sight z, the absorbance is[51]

$$\chi_{\text{gas}}(\lambda) = 1 - \exp\left[-\left(\sigma(\lambda)\int_0^{\ell} c(z)\mathrm{d}z\right)\right], \tag{49}$$

for gas concentration (i.e., number density) c and absorption cross-section σ. Equating the emissivity with the absorbance χ, the emitted radiance of a gas at uniform temperature is[52]

$$L_{\text{gas}}(\lambda) = \chi_{\text{gas}}(\lambda) L_{\text{bb}}(\lambda, T_{\text{gas}}). \tag{50}$$

When the gas is nonuniform in temperature, however, one must divide the gas cloud into a series of separate parcels, each with their own locally uniform temperature and their own local

absorption value (for light passing from one side to the other side of the parcel along the line of sight).[53–55] Although this substantially increases the complexity of the calculation, it is a straightforward process to model. In the unlikely case of a linear thermal gradient along the line of sight through the gas cloud, one reaches a result analogous to that of the linear gradient in a solid given in Eq. (46). What is different from solids is that most gases are weak absorbers/emitters, so that light can propagate through a large depth of gas before extinction. In addition, the lack of direct thermal conduction means that large differences in temperature between parcels of gas are possible. As a result, modeling a gas cloud as an isothermal body with uniform absorbance/emissivity via Kirchhoff's law is often subject to larger errors than in the case of solids.

8 Rough Surfaces and Scattering Media

So far we have considered only interfaces with smooth boundaries. When the boundaries are rough, incident light from one angle is scattered into a range of transmission and reflection angles, requiring a modification to the emissivity model that we have used so far. Jordan et al. provide an approach for doing this by modeling the orientation angle of the interface as comprising a probability distribution over angles.[18,56,57] In general, we can expect that, as the surface roughness becomes large, multiple reflections among surface facets increase, causing a reduction in reflectivity and a consequent increase in the emissivity.[14] The effect on emission polarization is more complex. Following Chang et al., we can model the emitting surface roughness as consisting of triangular corrugations of a given angle ϕ (see Fig. 11). From the standpoint of the viewer, the emission angle is θ', but the Fresnel equations for emission use the local surface normal to calculate the polarization properties. Thus, if the corrugations are ordered and not randomly oriented, this allows for polarized emission even at $\theta' = 0$, as shown in Fig. 11. For emission angles above the local tilt ϕ, the surface emission is affected by shadowing, in which part of the facet emits directly into the external medium, but emission from the remainder of the facet is reflected from the opposite face, inducing a change in polarization on reflection.[58,59] Although this shadowing effect makes analytical analysis of the problem difficult, numerical simulations have shown that the corrugation tends to increase overall emissivity, but the shadowing effect tends to reduce the degree of polarization in the emitted light.[18]

Goldstein and Chenault show polarimetric measurements of reflection from various paints for a range of angles of incidence.[60,61] Although the measurements were taken in the visible and near-infrared regions, they also contained very useful tables of the RMS surface roughness for each paint type, showing that the RMS roughness ranges from 50 nm for glossy paints to as much as 3 μm for matte paints.[62]

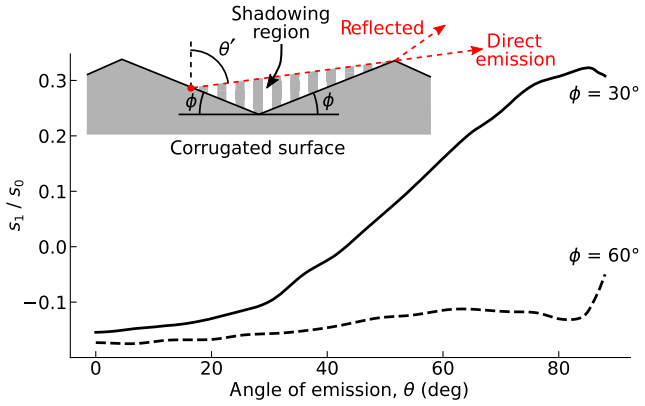

Fig. 11 Normalized linear polarization component of thermal emission from a corrugated surface with tilt angles of 30 deg and 60 deg. The behavior shown here is for out-of-plane viewing angles, at which the shadowing effect is irrelevant but reflection plays a role. (Inset) The emission geometry for a corrugated surface with facet tilts of ϕ and indicating the shadowed region that occurs for an emission angle of θ'. Light emitted from the shadowed region of the surface experiences reflection from the opposing facet. (Data for the curves shown here were obtained from Ref. 18.).

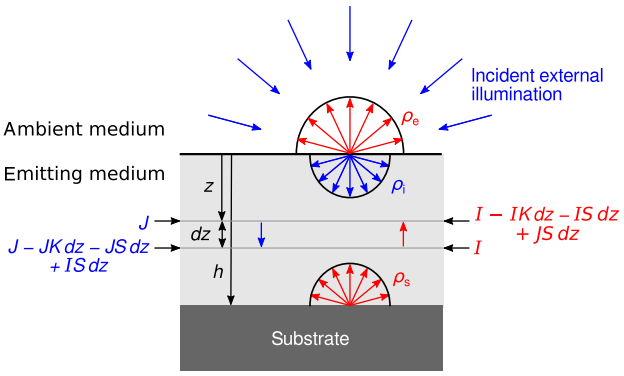

Fig. 12 Kubelka–Munk model of light propagation through a strongly scattering medium, showing upwelling flux I and a downwelling flux J in red and blue, respectively. The three reflectivities ρ_e, ρ_i, and ρ_s represent the hemispherical-average reflectivities for light reflecting at the boundary between two media.

Germer considers the effect of surface microroughness—surface scattering features that are small with respect to the light wavelength—and its effect on optical scattering and observed polarization.[63,64] Although Germer's simulations provide only for the case of visible light, the overall approach is equally applicable to infrared thermal emission and reflection and indicate that, because microroughness and subsurface defects have a somewhat different angular dependence of polarization, the two effects can be separated from one another with careful measurements. When a material is itself inhomogeneous, so that light propagating through the medium experiences a significant amount of scatter as it traverses the volume, the reflectivity and emissivity values calculated using a homogeneous material model are no longer reliable. One approach to take in this case is to form a Monte Carlo model of the rays propagating through the media, but this does not provide much physical insight to apply across various different media. When the scattering is large, however, we can take the diffuse light approximation, in which case we can apply the Kubelka–Munk approach to calculating the reflectivity.[65] In this approach, light is assumed to be evenly distributed in angle, so the calculated reflectivity is angle independent. This allows the problem to be simplified into a one-dimensional differential equation. Making use of the Kirchhoff law, we are then able to infer the emissivity from $\epsilon = 1 - \rho$.

In the diffuse light approach, we imagine the light as being composed of two streams, an upwelling flux I and a downwelling flux J (shown as red and blue, respectively, in Fig. 12). Each stream is subjected to absorption and scattering effects, for which we use coefficients K and S. If we examine the behavior of the two light streams as they traverse a layer of differential thickness dz inside the medium, we see that upwelling flux I suffers from absorption loss $(-IKdz)$ and scattering loss $(-ISdz)$ upon traversing the layer, but gains from backscattered downwelling light $(+JSdz)$. The downwelling flux J likewise suffers from absorption and scattering but gains from backscattered upwelling light. As a result, the differential changes in fluxes across the layer, defined as

$$\frac{dI}{dz} = \frac{I(z+dz) - I(z)}{dz}, \quad \frac{dJ}{dz} = \frac{J(z) - J(z+dz)}{dz}, \tag{51}$$

are given by the pair of coupled differential equations

$$\frac{dI}{dz} = -KI - SI + SJ, \quad \frac{dJ}{dz} = +KJ + SJ - SI. \tag{52}$$

The solutions for these equations are[45]

$$\left.\begin{aligned} I &= I_1(1-B)e^{Az} + I_2(1+B)e^{-Az} \\ J &= I_1(1+B)e^{Az} + I_2(1-B)e^{-Az} \end{aligned}\right\} \tag{53}$$

for

$$A = \sqrt{K(K+2S)}, \quad B = \sqrt{K/(K+2S)}, \tag{54}$$

and I_1, I_2 are constants to be determined by the boundary conditions of the problem.

Although the K and S coefficients are intended as experimentally determined parameters, researchers have established that in many cases we can approximate the absorption coefficient as $K \approx 2\alpha$ and the backscattering coefficient as $S \approx \sigma\eta$, where we model the medium as composed of discrete scatterers of scattering cross-section σ and number density η.[66,67] A more detailed calculation of K and S that takes into account specific material properties is presented in Refs. 68 and 69.

The steps toward calculating I_1 and I_2 are given in detail in Ref. 45, so we skip to the solution:

$$\rho = \rho_e + (1-\rho_e)(1-\rho_i)\frac{(1-B)Me^{Ah} - (1+B)Oe^{-Ah}}{MNe^{Ah} - OPe^{-Ah}}, \tag{55}$$

where

$$M = (1+B) - \rho_s(1-B), \tag{56}$$

$$N = (1+B) - \rho_i(1-B), \tag{57}$$

$$O = (1-B) - \rho_s(1+B), \tag{58}$$

$$P = (1-B) - \rho_i(1+B), \tag{59}$$

and ρ_e is the "external" reflectivity for light incident from the ambient medium onto the surface of the coating layer; ρ_i is the "internal" reflectivity for light incident on the surface of the coating layer from inside the coating; and ρ_s is the "substrate" reflectivity for light incident from the coating onto the substrate. The substrate itself is assumed to be fully opaque. Each of these three reflectivities ρ_e, ρ_i, and ρ_s are hemispherical average reflectivities obtained from the Fresnel equations. In the solution given in Eq. (55), the material reflectivity ρ is the diffuse reflectance, so it is independent of angle or polarization.

For a direct model of scattering media that does not derive the emissivity from applying Kirchhoff's law to the reflectivity, it becomes necessary to account for the emission density $j(\lambda, T)$ within the medium itself. Xu and Shen show that this adds a new source term to each of the equations in Eq. (53), requiring modification of the solution.[70]

9 Conclusion

One of the primary aims of this review was to gather together material illustrating how the elements in the theory of emission polarization can be derived from the Fresnel laws and volumetric blackbody radiation inside absorbing materials. We also considered the generalization of the Straubel theorem to absorbing materials, quantified the requirements for Kirchhoff's law to hold, and discussed the potential role of the mixed Poynting vector on emission. The physics of thermal emission is likely one of the few places in which the mixed Poynting vector may play a nontrivial role in practical measurement situations. Along the way through our survey, we also provided some of the answers to the questions that originally motivated gathering together the theory in one place. (Other answers await development until Part II of this review.) For example, we found that a layer of water fully obscures its underlying substrate when 1 mm thick or more. For hydrophilic surfaces in which water spreads widely without collecting into beads, water only forms layers this thick when it cannot drain. Wet surfaces that can drain retain only very thin layers of water, in which case the emission/reflection from the surface will be predominantly from the substrate and not the water layer.

We also found that high-emissivity paints can be considered to fully obscure their substrates when over about 10 μm thick, though this depends a lot on the type and density of colorants used in the paint. Surprisingly, a fully obscuring paint at visible wavelengths is generally a good guide that the paint will also be fully obscuring (or nearly so) in the thermal infrared as well.

There is, however, some concern about the use of paints for blackbody simulators. If the heater underneath the paint layer is pushed to a high temperature, so that the thermal gradient across the paint becomes large, this gradient can cause measurable deviations from Kirchhoff's law.

Finally, the McMahon–Gardon model of emission (Sec. 2) shows that the emission from a thin (partially transparent) plastic film is not simple. Most plastics have a complex absorption spectrum in the thermal infrared, particularly in the LWIR. Although some wavelengths are highly transparent, others are significantly absorbing, making their spectral dependence a major factor. In addition, any experimental measurements are prone to differences in composition and any coloring agents (such as carbon particles) or impurities. For example, clear plastic bags are more transparent in the infrared than black plastic bags because the latter contain a large concentration of absorbing carbon particles.

10 Appendix A: Gardon's Integral

In Sec. 2, we said that a 1D integral along the ray is sufficient to model the emissivity from a solid slab. We can confirm this with a rigorous treatment of the differential solid angle elements and the differential surface area element.

With the setup shown in Fig. 1, the volume element dV is part of an annular ring of radius r, with radial thickness dr and axial thickness dz. From the center of the ring, the elemental volume dV subtends an angle of $d\phi$. In cylindrical polar coordinates (r, ϕ, z), we write the elemental volume as

$$dV = r dr d\phi dz. \tag{60}$$

However, a more convenient representation is to rewrite this in terms of θ and $d\theta$ rather than r and dr. Using the triangle formed by r, z, and θ,

$$r = z \tan \theta. \tag{61}$$

The geometry shown in Fig. 1 gives

$$d\theta = ds/\ell = \frac{dr \cos \theta}{z/\cos \theta}, \tag{62}$$

so

$$dr = (z \cos^2 \theta) d\theta, \tag{63}$$

and

$$r dr = z^2 (\tan \theta / \cos^2 \theta) d\theta. \tag{64}$$

Therefore, in terms of the more convenient coordinates (z, ϕ, θ), the volume element is

$$dV = z^2 \frac{\sin \theta}{\cos^3 \theta} dz \, d\phi \, d\theta. \tag{65}$$

Again making use of the geometrical relationships shown in Fig. 1, we write the solid angle element $d\omega$, which is the solid angle subtended by surface area element dA from dV, as

$$d\omega = \frac{\text{projected area}}{\text{distance}^2} = \frac{dA \cos \theta}{\ell^2} = \frac{dA \cos \theta}{z^2/\cos^2 \theta} = dA \frac{\cos^3 \theta}{z^2}. \tag{66}$$

Similarly, for the solid angle element $d\Omega$ defined within the blue lines drawn in Fig. 1(b) representing the solid angle subtended by dV from dA, we have

$$d\Omega = \frac{\text{projected area}}{\text{distance}^2} = \frac{\cos \theta r dr \, d\phi}{\ell^2} = \sin \theta d\theta \, d\phi. \tag{67}$$

The element of volume dV emits power dP in the direction of dA:

$$dP = jdVd\omega. \tag{68}$$

The power arriving at dA from dV is less than this because of absorption along the path. Including path absorption, we have

$$dP = je^{-kz/\cos\theta}dVd\omega. \tag{69}$$

The corresponding elemental radiance reaching the surface from inside the solid is given by the power dP per units area dA per unit solid angle $d\Omega$:

$$dL = dP/(dA\,d\Omega). \tag{70}$$

With this expression, we can solve for the radiance arriving at dA from within the solid by integrating over all layers:

$$L = \int_{z=0}^{z=\infty} \frac{dP}{dAd\Omega}\mathrm{d}z = \int_0^\infty \frac{je^{-kz/\cos\theta}dV\,d\omega}{dA[\sin\theta d\theta\,d\phi]}\mathrm{d}z = j\int_0^\infty e^{-kz/\cos\theta}\mathrm{d}z. \tag{71}$$

Acknowledgments

The author is grateful to Photron Inc. for allowing the use of their FLIR x6900sc InSb camera in the MWIR polarimetry experiments. The author would also like to thank Shuhei Shibata for help with conducting the FLIR A35 LWIR polarimetry experiments. A portion of this research was funded by a grant from Denso Corp. and by JSPS KAKENHI (Grant No. JP 20K04516).

References

1. R. A. Millikan, "A study of the polarization of the light emitted by incandescent solid and liquid surfaces," *Phys. Rev.* **3**, 81–99 (1895).
2. R. A. Millikan, "A study of the polarization of the light emitted by incandescent solid and liquid surfaces. II," *Phys. Rev.* **3**, 177–192 (1895).
3. H. O. McMahon, "Thermal radiation from partially transparent reflecting bodies," *J. Opt. Soc. Am.* **40**, 376–380 (1950).
4. R. Gardon, "The emissivity of transparent materials," *J. Am. Ceram. Soc.* **39**, 278–285 (1956).
5. O. Sandus, "A review of emission polarization," *Appl. Opt.* **4**, 1634–1642 (1965).
6. J. S. Tyo et al., "The effects of thermal equilibrium and contrast in LWIR polarimetric images," *Opt. Express* **15**, 15161–15167 (2007).
7. R. Straubel, "Über einen allgemeinen Satz der geometrischen Optik und einige Anwendungen [About a general theorem of geometrical optics and some applications]," *Verhandl. Deut. Physik. Ges.* **4**, 328–334 (1902).
8. A. Gershun, "The light field," *J. Math. Phys.* **18**, 51–151 (1939).
9. R. J. Bell et al., "Generalized laws of refraction and reflection," *J. Opt. Soc. Am.* **59**, 187–189 (1969).
10. J. Kischkat et al., "Mid-infrared optical properties of thin films of aluminum oxide, titanium dioxide, silicon dioxide, aluminum nitride, and silicon nitride," *Appl. Opt.* **51**, 6789–6798 (2012).
11. G. M. Hale and M. R. Querry, "Optical constants of water in the 200-nm to 200-μm wavelength region," *Appl. Opt.* **12**, 555–563 (1973).
12. S. Popova, T. Tolstykh, and V. Vorobev, "Optical characteristics of amorphous quartz in the $1400-200\ \mathrm{cm}^{-1}$ region," *Opt. Spectrosc.* **33**, 444–445 (1972).
13. M. R. Querry, "Optical constants," U. S. Army CRDC, CRDC-CR-85034 (1985).
14. U. P. Oppenheim and Y. Feiner, "Polarization of the reflectivity of paints and other rough surfaces in the infrared," *Appl. Opt.* **34**, 1664–1671 (1995).

15. A. D. Rakic, "Algorithm for the determination of intrinsic optical constants of metal films: application to aluminum," *Appl. Opt.* **34**, 4755–4767 (1995).
16. O. S. Heavens, *Optical Properties of Thin Solid Films*, Dover (1991).
17. D. H. Goldstein, *Polarized Light*, 2nd ed., Marcel Dekker (2003).
18. P. C. Y. Chang et al., "Importance of shadowing and multiple reflections in emission polarization," *Waves Rand. Media* **12**(1), 1–19 (2002).
19. S. J. Orfanidis, "Electromagnetic waves and antennas," https://www.ece.rutgers.edu/~orfanidi/ewa/ (2016).
20. S. J. Byrnes, "Multilayer optical calculations," https://arxiv.org/abs/1603.02720 (2016).
21. F. L. Pedrotti, L. M. Pedrotti, and L. S. Pedrotti, *Introduction to Optics*, 3rd ed., Cambridge University Press (2018).
22. J. A. Shaw, "Degree of linear polarization in spectral radiances from water-viewing infrared radiometers," *Appl. Opt.* **38**, 3157–3165 (1999).
23. M. A. Dupertuis, B. Acklin, and M. Proctor, "Generalized energy balance and reciprocity relations for thin-film optics," *J. Opt. Soc. Am. A* **11**, 1167–1174 (1994).
24. G. P. Ortiz and W. L. Mochán, "Nonadditivity of Poynting vector within opaque media," *J. Opt. Soc. Am. A* **22**, 2827–2837 (2005).
25. H. A. Macleod, *Thin Film Optical Filters*, 3rd ed., Institute of Physics, Philadelphia (2001).
26. H. Weber, "The Fresnel equations for lossy dielectrics and conservation of energy," *J. Mod. Opt.* **61**, 1219–1224 (2014).
27. J. F. Lodenquai, "Electromagnetic wave propagation in media with complex refractive indices and transmission through absorbing films," *Am. J. Phys.* **59**, 248–254 (1991).
28. F. R. Keßler, "Optics with gradients of free carrier concentration," in *Festkörperprobleme*, P. Grosse, Ed., Vol. **26**, pp. 277–308, Springer (1986).
29. C. von Fragstein, "History of the mixed Poynting vector," *Abh. Braunschw. Wiss. Ges.* **34**, 25–29 (1987).
30. A. MacLeod, "The mixed Poynting vector," *Soc. Vac. Coat. Bull.* **14**(Summer), 30–34 (2014).
31. N. Sun et al., "Effects of non-synchronized variations of electric and magnetic properties on transmitted waves at lossy interface," *J. Quantum Spectrosc. Radiat. Transf.* **138**, 50–59 (2014).
32. J. R. Howell, R. Siegel, and M. P. Mengüç, *Thermal Radiation Heat Transfer*, 5th ed., CRC Press (2010).
33. S. Edalatpour and M. Francoeur, "Size effect on the emissivity of thin films," *J. Quant. Spectrosc. Radiat. Transf.* **118**, 75–85 (2013).
34. R. O. Carter, III, "The effect of metal optical constants on far- and mid-infrared reflection-absorption," *Spectrochim. Acta A* **47**, 551–561 (1991).
35. E. D. Palik, ed., *Handbook of Optical Constants of Solids*, Vol. 1, Academic Press (1998).
36. J. D. Bernardin et al., "Contact angle temperature dependence for water droplets on practical aluminum surfaces," *Int. J. Heat Mass Transf.* **40**, 1017–1033 (1997).
37. B. M. Gallaway et al., "Influence of water depths on friction properties of various pavement types," Texas Transportation Institute, 2-8-69-138 (1974).
38. N. F. Mott, "Oxidation of metals and the formation of protective films," *Nature* **145**, 996–1000 (1940).
39. R. Raman and H. K. Sehgal, "Emissivity of substrate supported films," *Energy Convers. Manage.* **22**, 213–217 (1982).
40. G. Neuer and F. Guntert, "*In situ* measurements of layer thickness during oxidation of titanium," *Thermochim. Acta* **133**, 299–304 (1988).
41. P. Pigeat, D. Rouxel, and B. Weber, "Calculation of thermal emissivity for thin films by a direct method," *Phys. Rev. B* **57**, 9293–9300 (1998).
42. K. Richter, G. Chen, and C.-L. Tien, "Partial coherence theory of multilayer thin-film optical properties," *Opt. Eng.* **32**, 1897–1903 (1993).
43. C. F. Anderson and Y. Bayazitoglu, "Radiative properties of films using partial coherence theory," *J. Thermophys. Heat Transf.* **10**, 26–32 (1996).
44. A. H. Madjid, "Spectral emissivity of nonisothermal semi-infinite slabs of transparent materials," *J. App. Phys.* **44**, 5423–5426 (1973).

45. J. C. Richmond, "Relation of emittance to other optical properties," *J. Res. NIST* **67**, 217–226 (1963).
46. A. R. Korb, J. W. Salisbury, and D. M. D'Aria, "Thermal-infrared remote sensing and Kirchhoff's law 2. Field measurements," *J. Geophys. Res. B* **104**, 15339 (1999).
47. A. E. Wechsler and P. E. Glaser, "Pressure effects on postulated lunar materials," *Icarus* **4**, 335–352 (1965).
48. L. Millán, I. Thomas, and N. Bowles, "Lunar regolith thermal gradients and emission spectra: modeling and validation," *J. Geophys. Res. E* **116**, 12003 (2011).
49. M. Hori et al., "Modeling angular-dependent spectral emissivity of snow and ice in the thermal infrared atmospheric window," *Appl. Opt.* **52**, 7243–7255 (2013).
50. M. A. Weinstein, "On the validity of Kirchhoff's law for a freely radiating body," *Am. J. Phys.* **28**, 123–125 (1960).
51. C. F. Bohren and E. E. Clothiaux, *Fundamentals of Atmospheric Radiation*, Wiley (2006).
52. S. E. Golowich and D. G. Manolakis, "Performance limits of LWIR gaseous plume quantification," *Proc. SPIE* **8048**, 80481F (2011).
53. K. Stamnes et al., "Numerically stable algorithm for discrete-ordinate-method radiative transfer in multiple scattering and emitting layered media," *Appl. Opt.* **27**, 2502–2509 (1988).
54. G. E. Thomas and K. Stamnes, *Radiative Transfer in the Atmosphere and Ocean*, Cambridge (1999).
55. N. Hagen, "Survey of autonomous gas leak detection and quantification with snapshot infrared spectral imaging," *J. Opt.* **22**, 103001 (2020).
56. D. L. Jordan, G. D. Lewis, and E. Jakeman, "Emission polarization of roughened glass and aluminum surfaces," *Appl. Opt.* **35**, 3583–3590 (1996).
57. J. A. Shaw and C. Marston, "Polarized infrared emissivity for a rough water surface," *Opt. Express* **7**, 375–380 (2000).
58. B. G. Smith, "Geometrical shadowing of a random rough surface," *IEEE Trans. Antennas Propag.* **15**(5), 668–671 (1967).
59. J. A. Ogilvy, "Wave scattering from rough surfaces," *Rep. Prog. Phys.* **50**, 1553–1608 (1987).
60. D. H. Goldstein and D. B. Chenault, "Spectropolarimetric reflectometer," *Opt. Eng.* **41**, 1013–1020 (2002).
61. D. H. Goldstein, "Polarization measurements of automobile paints," *Proc. SPIE* **6972**, 69720V (2008).
62. D. H. Goldstein, "Polarimetric characterization of federal standard paints," *Proc. SPIE* **4133**, 112–122 (2000).
63. T. A. Germer, "Angular dependence and polarization of out-of-plane optical scattering from particulate contamination, subsurface defects, and surface microroughness," *Appl. Opt.* **36**(33), 8798–8805 (1997).
64. T. A. Germer and C. C. Asmail, "Polarization of light scattered by microrough surfaces and subsurface defects," *J. Opt. Soc. Am. A* **16**(6), 1326–1332 (1999).
65. P. Kubelka, "New contributions to the optics of intensely light-scattering materials. Part I," *J. Opt. Soc. Am.* **38**, 448–457 (1948).
66. P. S. Mudgett and L. W. Richards, "Multiple scattering calculations for technology," *Appl. Opt.* **10**, 1485–1502 (1971).
67. J. H. Nobbs, "Kubelka–Munk theory and the prediction of reflectance," *Rev. Prog. Coloration Rel. Top.* **15**, 66–75 (1985).
68. L. Liu et al., "Calculation of emittance of a coating layer with the Kubelka–Munk theory and the Mie-scattering model," *J. Opt. Soc. Am. A* **22**, 2424–2429 (2005).
69. M. P. Diebold, *Application of Light Scattering to Coatings: A User's Guide*, Springer (2014).
70. W. Xu and S. C. Shen, "Infrared radiation and reflection in an inhomogeneous coating layer on a substrate," *Appl. Opt.* **31**, 4488–4496 (1992).

Biography of the author is not available.